RSC Advances

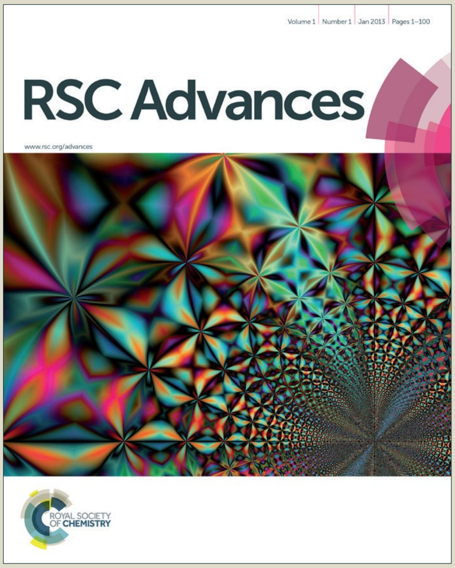

ROYAL SOCIETY OF CHEMISTRY

www.rsc.org/advances

Aerosol Assisted Chemical Vapour Deposition of a ZrO_2-TiO_2 Composite Thin Film with Enhanced Photocatalytic Activity

Abdullah M. Alotaibi[1], Sanjayan Sathasivam[1,2], Ivan P. Parkin[1]*

*Corresponding author

[1]Materials Chemistry Centre, Department of Chemistry, University College London, 20 Gordon Street, London WC1H 0AJ, UK

Fax: (+44) 20-7679-7463

E-mail: i.p.parkin@ucl.ac.uk

[2]Bio Nano Consulting Ltd, The Gridiron Building, One St. Pancras Square, London N1C 4AG, UK

Fax: (+44) 20-7396-1056

Abstract

ZrO_2-TiO_2 composite thin films were deposited by aerosol assisted chemical vapour deposition onto a glass substrate at 450 °C and then annealed at 600 °C. For comparison ZrO_2 thin films and TiO_2 thin films were deposited under the same conditions. X-ray diffraction (XRD), scanning electron microscopy (SEM), energy dispersive X-ray spectroscopy (EDX), X-ray photoelectron spectroscopy (XPS), UV-Vis and Raman spectroscopy were used to characterize all films. Photocatayltic activities were tested by degradation of intelligent ink containing resazurin redox dye under UVA irradiation. The formal quantum efficiency (FQE) and yield (FQY) for the ZrO_2-TiO_2 composite thin films were determined as 2.03×10^{-3} dye molecules per incident photon and 4.91×10^{-3} dye molecules per absorbed photon respectively. Surprisingly the ZrO_2 – TiO_2 composite was a more efficient photocatalyst than the comparable TiO_2 coating.

1. Introduction

Titanium dioxide (TiO_2) is a well-known and highly versatile semiconducting material with applications in gas-sensing, photovoltaics and anti-microbial devices.[1-5] It is also the best established and most widely used photocatalyst due to its relatively high photo-activity compared other similar semiconductors (ZnO) and its chemical stability.[6, 7] It has been commercialised for use in self-cleaning windows and the current market worth over £ 1.5 billion at the distributor level.

TiO_2 exists in three common phases - anatase, rutile and brookite. The anatase phase is considered the most photocatalytically active due to its more efficient transport of bulk excitons to the surface and the indirect bandgap that enables longer exciton lifetimes.[4, 8] However, the wide bandgap of anatase TiO_2 means that it is transparent to visible light and hence much of the solar spectrum is not absorbed, resulting in sub-optimum photocatalytic activity.[3, 9, 10] Efforts to enhance the photoactivity of TiO_2 involve doping with anionic species such as fluorine, nitrogen and sulphur to decrease the bandgap to the visible region.[3, 10, 11] Furthermore, photocatalytic activity in anatase is also hindered by the recombination of excitons before they migrate to the surface where they can carry out useful work.[1] Recombination can be reduced by composite formation with other metal oxides that act as electron or hole sinks due to favourable band positions.[12-14] Furthermore, composite formation results in surface hydroxyl groups that accept holes after irradiation and enable spatial separation of charger carriers and hence reduce recombination.[12, 15] Composite formation also enhances crystallinity and increases surface area, two properties that are important for high photocatalytic activity.[16]

Zirconium oxide, ZrO_2, is an important material with applications in fuel cells[17-19], gas sensors[20], optical-dielectrics[21] and antimicrobial coatings[22]. It is generally synthesised *via* sol-gel[23, 24], hydrothermal[25] and solid-state reactions. Thin films have also been produced *via* metal-organic CVD[26, 27] and pulsed laser deposition[28, 29]. ZrO_2 crystallises in the monoclinic, tetragonal or cubic structure depending on the temperature. Monoclinic ZrO_2 that is observed under ambient conditions converts to the tetragonal form above 1150 ^oC and above 2300 ^oC to the cubic phase. However there are literature reports of lower temperature cubic ZrO_2 synthesis that involve the use dopant amounts of yttrium or calcium as stabilisers. Furthermore, Prakashbabu *et at.* have shown the formation of cubic ZrO_2 nanopowders at 400 ^oC without the need for a stabilising agent.[30]

Composite ZrO_2-TiO_2 material has applications as catalysts/catalyst supports in many reactions, gas sensors and photoconductive thin films. Synergistic effects arising coupling of ZrO_2 with TiO_2 is known to enhance the latters photocatalytic properties. Furthermore, it has been previously noted that ZrO_2-TiO_2 composites (as well as other binary oxide systems) have an increased surface acidity and hence reactivity compared to pure TiO_2.[31] Increased surface acidity in such systems is thought to derive from greater amounts of surface hydroxyl groups. These groups trap photo-induced holes and enhance photocatalytic activity by reducing electron-hole pair recombination. Furthermore, as the hydroxyl groups are concentrated on the surface, the holes are trapped near the surface hence it allows efficient oxidation of pollutant molecules directly or *via* the formation of hydroxyl radicals.[31, 32]

In this paper we report the first preparation of ZrO_2-TiO_2 composite thin films via aerosol assisted chemical vapour deposition (AACVD). AACVD is a simple and easily tuneable CVD technique that has been employed to fabricate photocatalytic, optoelectronic and photocoltaic films.[33-38] In AACVD the precursors are dissolved in a suitable solvent, then the solution is atomised and transported into the deposition chamber using a carrier gas. Compared to other solution based methods like sol-gel techniques (which is often a multistep process) where coating large areas can be an issue, AACVD is a single step technique that is easily scalable.[39, 40]

The composite film was made along with pure ZrO_2 and TiO_2 under the same conditions for comparison. The photocatalytic properties of the films under UVA irradiation showed the composite to have superior activity.

2. Experimental

2.1. Materials

Zirconium acetylacetonate [Zr(acac)$_4$] and titanium isopropoxide [Ti(OCH(CH$_3$)$_2$)$_4$] were purchased from Sigma-Aldrich Chemical Co; absolute ethanol from Merck Chemicals. All chemicals were used as received.

2.2. Precursors solution for AACVD

Three types of films were prepared, ZrO_2-TiO_2 composite, ZrO_2 and TiO_2. For the composite, (1 mmol = 0.48 g) of [Zr(acac)$_4$] was dissolved into 40 ml of absolute ethanol and (1 mmol ≈ 0.30 ml) of [Ti(OCH(CH$_3$)$_2$)$_4$] was added to [Zr(acac)$_4$] and left to stir 30 minutes before use by AACVD. For the ZrO_2 film, (1 mmol = 0.48 g) of [Zr(acac)$_4$] was dissolved into 40 ml of absolute ethanol and added to a humidifier flask (100 mL). For TiO_2, ≈ 0.30 ml of [Ti(OCH(CH$_3$)$_2$)$_4$] was dissolved at 40 ml of absolute ethanol then added to the humidifier flask (100 mL).

2.3. Aerosol assisted chemical vapour deposition (AACVD)

Aerosol assisted chemical vapour deposition (AACVD) was used to deposition the films. The reactor contained a carbon block, containing a Whatmann cartridge heater. A Pt–Rh thermocouple was used to control the temperature on the substrate. The reactor has top and bottom plates for deposition and the top plate was placed 8 mm above the substrate. The aerosol mist was generated by a PicoHealth^{TM} ultrasonic humidifier at room temperature. The deposition was carried out on SiO_2 coated float-glass, this prevented diffusion of ions from the glass into the film as it acted as a blocking layer. Prior to use the glass was washed with water, acetone and isopropanol and allowed to dry in the oven at 100 °C. Depositions were carried out in a cold-walled horizontal-bed CVD reactor at 450 °C. The deposition was conducted by generation of an aerosol and using nitrogen (flow rate 1.4 L min$^-$) to drive the aerosol into reactor, this took about 40-45 minutes for all the precursors to transfer. When the deposition was completed, the heat was turned off and the glass was left to cool under nitrogen to room temperature. The glass substrates were handled in air and annealed at 600 °C for one hour.

2.4. Films characterization

XRD data were collected using a microfocus Bruker GAADS powder X-ray diffractometer using a monochromated Cu Kα radiation. (XPS) X-ray photoelectron spectroscopy was carried out using a Thermo Scientific K-Alpha instrument with monochromatic Al-Kα source. Raman spectroscopy was obtained from a Renishaw 1000 spectrometer equipped with a 514.5 nm laser. SEM images were carried out on a JEOL 6301F instrument with acceleration voltage of 5 kV. Samples were prepared by cutting to 10 mm × 10 mm and then coated with gold in order to avoid charging. UV-Vis spectroscopy was carried out using both a Lamda 25 and 950 instruments. Water droplet contact angles were carried out using an FTA-1000 drop shape instrument. A Fujifilm Finepix HS25 EXR camera captured image at 1000 frames per second.

2.5. Photocatalytic test

Prior to photocatalytic testing the samples were cleaned with distilled water, rinsed in isopropanol and acetone and placed under UVC light to irradiate for 30 minutes to activate the surface. The photocatalyic activity was measuring using a resazurin based “intelligent ink” devised by Mills and *et al*.[41] Surfaces of the films were covered evenly with the dye. Photocatalytic reduction of the dye by UVA light was measured by UV-Vis spectroscopy. The formal quantum efficiency (FQE) was calculated by dividing the rate of dye molecules destroyed by the photon flux. The formal quantum yield (FQY) was calculated as a UVX radiometer with a detector for 365 nm radiation was used to measure the photon flux and photon absorption for each film.

2.6. Synthesis of ‘intelligent ink’

Resazurin (92%), hydroxy ethyl cellulose and Glycerol (99.6%) were all purchased from Sigma-Aldrich Chemical Co.

40 mg of resazurin redox dye added to 40 ml of aqueous solution and added 3 g of glycerol, 0.45 g of d hydroxylethyl cellulose. That was placed one day in the fridge between 3-5 °C for one day.[41]

3. Result and discussion

Aerosol assisted chemical vapour deposition (AACVD) was used to deposit TiO_2, ZrO_2 and ZrO_2-TiO_2 composite films on glass substrates at 450 °C. The samples were then annealed at 600 °C for one hour. The pure TiO_2 and ZrO_2 films were deposited from $[Ti(OCH(CH_3)_2]_4$/ethanol and [Zr(acac)4]/ethanol solution respectively. The composite ZrO_2-TiO_2 films were synthesised from the one-pot molar equivalent ethanol solution of $[Zr(acac)_4]$ and $[Ti(OCH(CH_3)_2]_4$. All films were translucent with interference fringes indicating a variation in thickness along the substrate. The films also passed the Scotch^{TM} tape test and were indefinitely stable under visible light and in air.

3.1 Material characterisation

A range of techniques were used to characterize and understand the material and functional properties of the ZrO_2-TiO_2 thin films.

3.1.1 X-ray diffraction

Figure 1 shows the XRD patterns of the ZrO_2, TiO_2 and ZrO_2-TiO_2 composite films are deposited by AACVD along with the standard patterns of ZrO_2 and TiO_2. The ZrO_2 films surprisingly match the high temperature cubic phase with reflections for the (111), (200), (220) and (311) planes at 2θ values of 30.3, 35.3, 50.6 and 60.3^o respectively. Although the formation of the cubic phase below 2300 ^{o}C is not common without the use of stabilisers there are sporadic literature examples of cubic ZrO_2 formation at temperatures as low as 400 ^{o}C.[30] The TiO_2 film was pure anatase with reflection at (101), (112), (200) and (204) at 2θ values of 25.3, 38.6, 48.0, 55.1 and 62.8^o. XRD pattern for ZrO_2-TiO_2 composite films showed a dual phase system corresponding to cubic ZrO_2 with the (111) at 30.9 2θ and TiO_2 anatase with reflections corresponding to the expected (101), (200) and (211) planes.

Applying the Debye - Scherrer formula to the diffraction data showed that the TiO_2 film was made up of crystallites almost twice and four times the size as those found in the ZrO_2 and ZrO_2 – TiO_2 composite films respectively (see supporting information).[42]

Furthermore, the peaks from the composite film show shifts towards lower 2θ values for the anatase phase and to higher 2θ for the cubic ZrO_2 phase indicating some formation of a solid solution. The shift to lower 2θ values of the anatase phase indicates an expansion of the TiO_2 unit cell due to the substitutional replacement of Ti^{4+} (ionic radii 0.60 Å) with the larger Zr^{4+}

(ionic radii 0.72 Å) ions. This has previously been observed (via both XRD and EXAFS experiments) for Zr doped anatase TiO_2.[43, 44] Conversely the peaks corresponding to the ZrO_2 cubic phase are shifted to higher *2θ* values, which is evident of a contraction in the ZrO_2 unit cell. There is further evidence for solid solution formation in the composite ZrO_2-TiO_2 film from the Raman data shown below.

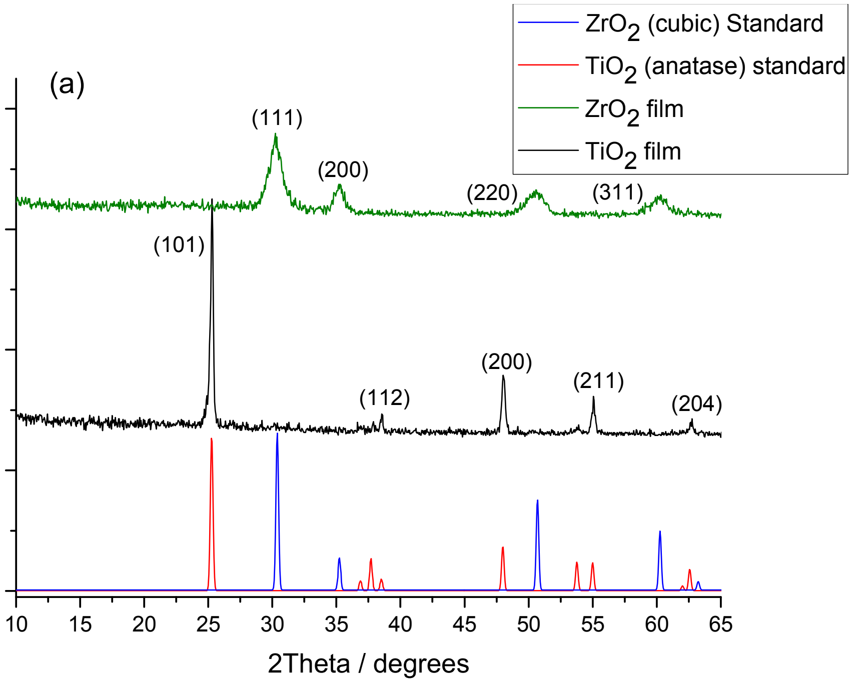

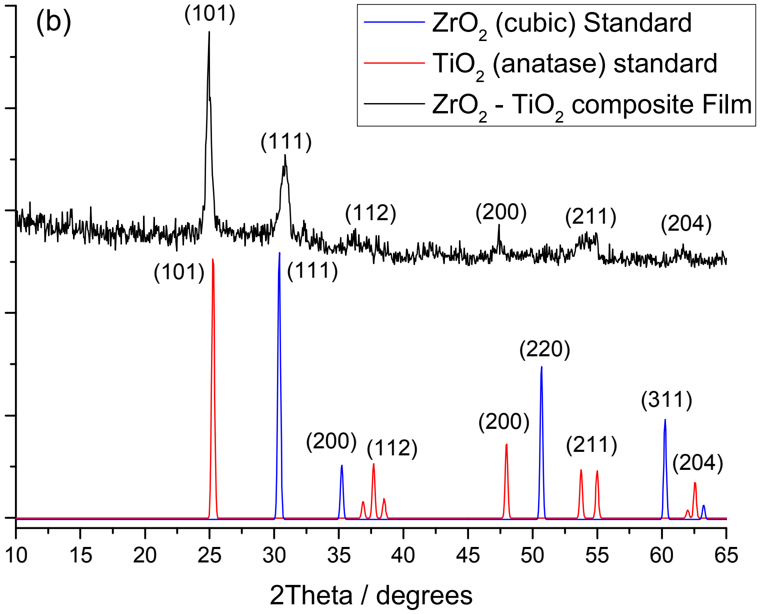

Figure 1: Shows XRD for a) ZrO_2 and TiO_2 and b) ZrO_2-TiO_2 composite thin films grown by AACVD from $[Ti(OPr^i)_4]$ and $[Zr(acac)_4]$ in ethanol carrier solvent at 450 °C followed by annealed at 600 °C for 1 hour.

3.1.2 Raman spectroscopy

Raman spectra for TiO_2, and ZrO_2-TiO_2 composite thin films are shown in Figure 2. The spectrum for the anatase TiO_2 (figure 3) film showed peaks at 143 cm^{-1} for (E_g, strong peak), 198 cm^{-1} for (E_g, weak peak), 396 cm^{-1} for (B_{1g}), 517 cm^{-1} for (A_{1g}, B_{1g}) and 638 cm^{-1} for (E_g) matching well with literature values.[45] The ZrO_2-TiO_2 composite thin film (Figure 2) gave a spectrum corresponding to the anatase phase of TiO_2 again with peaks at 138, 389, 514 and 632 cm^{-1}. Interestingly, the principal Eg peak in the ZrO_2-TiO_2 composite film was blue shifted to 138 cm^{-1} corresponding to an expansion in the TiO_2 unit cell due to some substitutional doping of Ti^{4+} with Zr^{4+} in the TiO_2 matrix as also seen from the XRD analysis (Figure 1).[46]

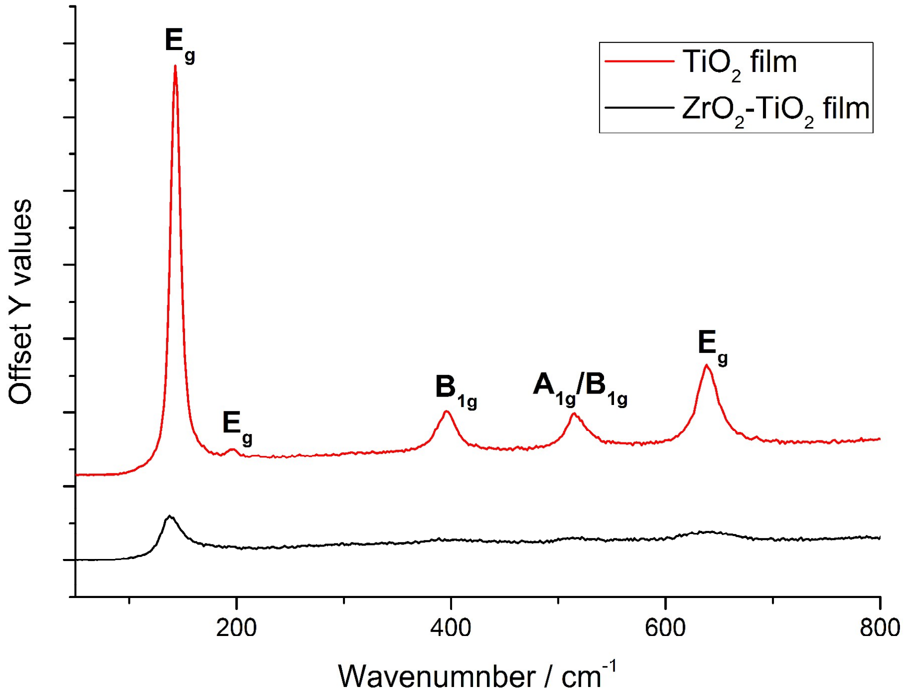

Figure 2: Shows the Raman spectra for a) TiO_2 and b) ZrO_2-TiO_2composite thin films grown by the AACVD.

3.1.3 X-ray photoelectron spectroscopy (XPS)

XPS was preformed on the ZrO_2-TiO_2 composite film to determine the oxidation states of the Zr and Ti (Figure 3). The Zr $3d_{5/2}$ peak appeared at 182.5 eV with Ti $2p_{3/2}$ peak at 459.2 eV corresponding to Zr and Ti in the 4+ oxidation state as expected.[44] There were two oxygen environments detected that matched chemisorbed oxygen (at 531.4 eV) and oxygen bound to Zr and Ti (529.5 eV) (See supporting information).[47] XPS also showed the ratio of Zr : Ti on the surface of the composite film was 1 : 4 and bulk analysis using energy dispersive X-ray spectroscopy (EDX) found the overall ratio to be 1 : 2.7 therefore showing that the composite film was rich in Ti with surface segregation of Ti also occurring. This was in spite of equimolar quantities of both precursors being used in the AACVD system hence it suggest that the $[Ti(OCH(CH_3)_2)_4]$ is a more efficient CVD precursor at the deposition temperature (500 °C) compared to $[Zr(acac)_4]$. This has been previously observed for other related Ti containing composite systems grown *via* AACVD.[13]

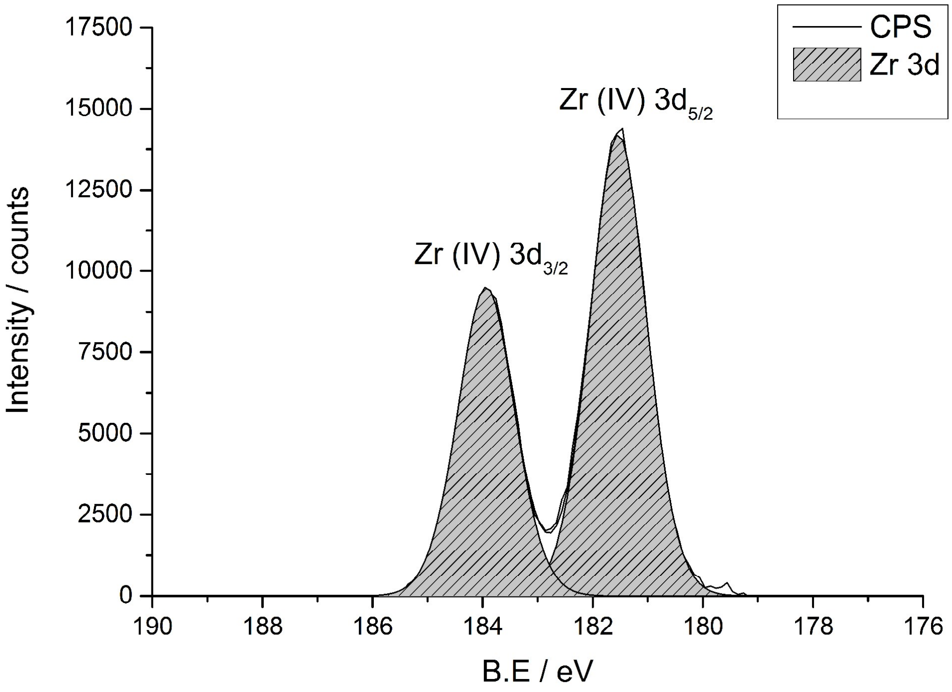

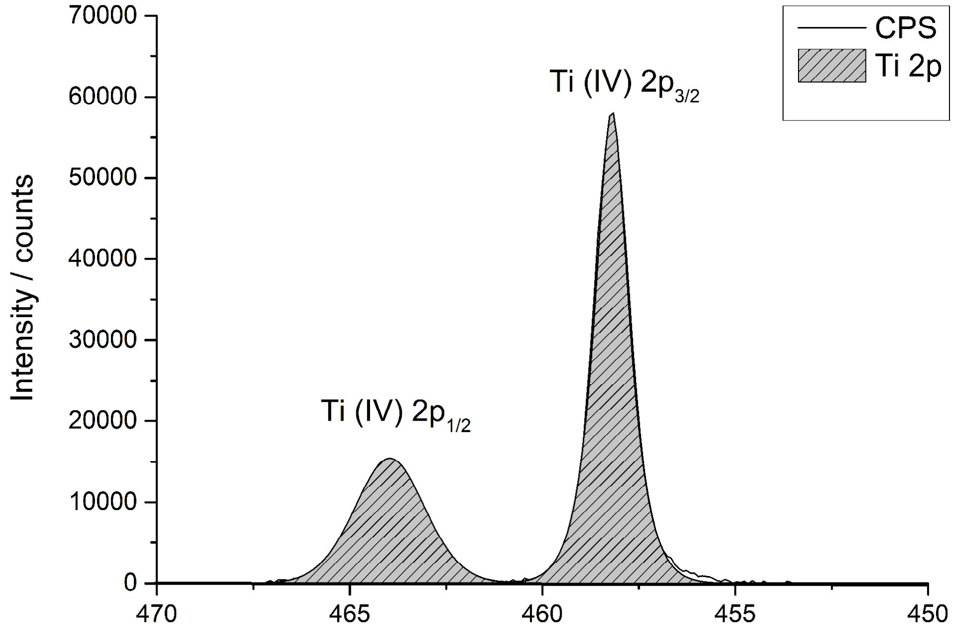

Figure 3: XPS spectra of ZrO_2-TiO_2 composite thin film showing the Ti $2p_{3/2}$ and $2p_{1/2}$ transitions (above) and Zr $3d_{5/2}$ and $3d_{3/2}$ transitions (below).

3.1.4 Scanning electron microscopy (SEM)

The mophology of the AACVD deposited thin films (Figure 4) was analysed by scanning electron microspy (SEM). The morphology of the ZrO_2 film consists of domes ranging from 100 to 500 nm in diameter on an otherwise flat surface (Figure 4a). The pure TiO_2 film however is made up of a dense array of facets that are on average 400 nm long (Figure 4b). Composite formation of these two system results in a surface morphology made up of densly packed partilces (ca. 50 nm wide) and like in the pure ZrO_2 film, the composite film also contains domes that are almost a micron wide that appear cracked (Figure 4c). Side on images (Figure 4d-f) indicate the thickness of the ZrO_2 and TiO_2 films to be ca. 250 nm whereas the composite film was almost 500 nm as expected.

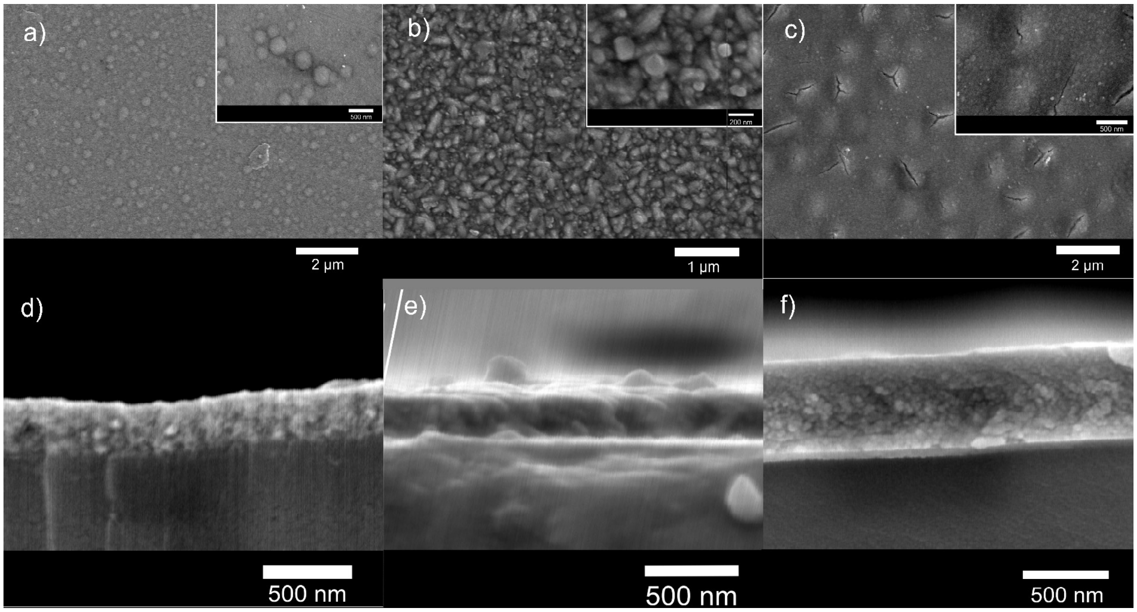

Figure 4: SEM images of the a) ZrO_2, b) TiO_2 and c) ZrO_2 – TiO_2 composite films with the high magnification images inset. The side on images - d) ZrO_2, e) TiO_2 and f) ZrO_2 - TiO_2 composite – show the film thickness.

3.1.5 UV-visible measurements (UV-Vis)

Figure 4 illustrates UV-Vis transmission spectrum for TiO_2, ZrO_2 and ZrO_2-TiO_2 composite thin films. All films show interference fringes that are expected for ZrO_2 and TiO_2 based films. The transparency of the ZrO_2-TiO_2 composite thin film is between 60 and 70% in the visible region (380–760 nm) and near infrared region (760–2500 nm). This is slightly lower than the transparency values obtained for pure ZrO_2 and TiO_2 films, which were between 80 and 90% again in both the visible and infrared regions. Reflectance measurements shown in Figure 5 (b) show that the composite film has higher reflectance (between 35 and 45%) than the pure films, which is at 10% and 25% for ZrO_2 and TiO_2 respectively.

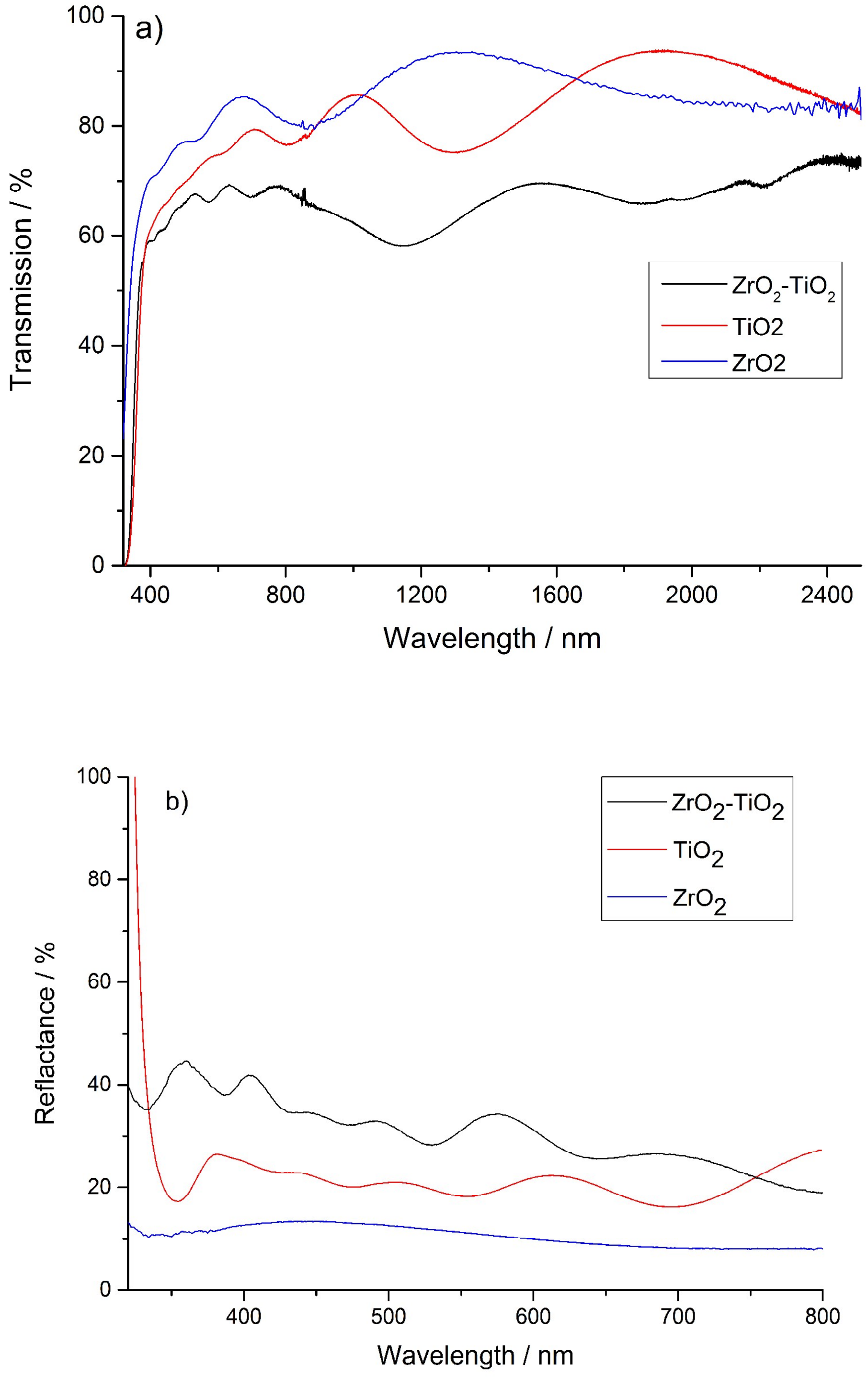

Figure 5: Illustrates a) transmittance and b) reflectance spectra of ZrO_2, TiO_2 and ZrO_2-TiO_2 composite thin films

The indirect optical bandgaps of the TiO_2 and ZrO_2-TiO_2 composite thin films were calculated using the Tauc plot (see supporting information). The anatase TiO_2 film gave a bandgap of 3.2 eV matching literature values whereas the determination of the ZrO_2 film's bandgap was not possible due to absorption from the glass substrate in the UV-Vis spectrum. For the composite film a bang gap of 3.3 eV was calculated owing to the anatase component of the film.

3.2 Functional testing

3.2.1 Photocatalysis testing

The photocatalytic study of the TiO_2 and ZrO_2-TiO_2 thin films were determined under the same condition by the resazurin dye (intelligent ink) under 365 nm UV light irradiation. The photoreduction reaction was induced by UVA radiation (flux = 3.67×10^{14} photons per cm^2 per s) and observed by UV-Vis spectroscopy. The photocatalytic activity of the pure ZrO_2 was not tested due to the inability of UVA radiation to activate the ZrO_2 due to its wide bandgap. The rate of dye degradation on the TiO_2 film was 3.3×10^{-4} dye molecules cm^{-2} s^{-1} taking for the resazurin that is a royal blue colour to be photoreduced to the pink resorufin. The composite film showed a degradation rate an order of magnitude better (2.0×10^{-3} dye molecules cm^{-2} s^{-1}).

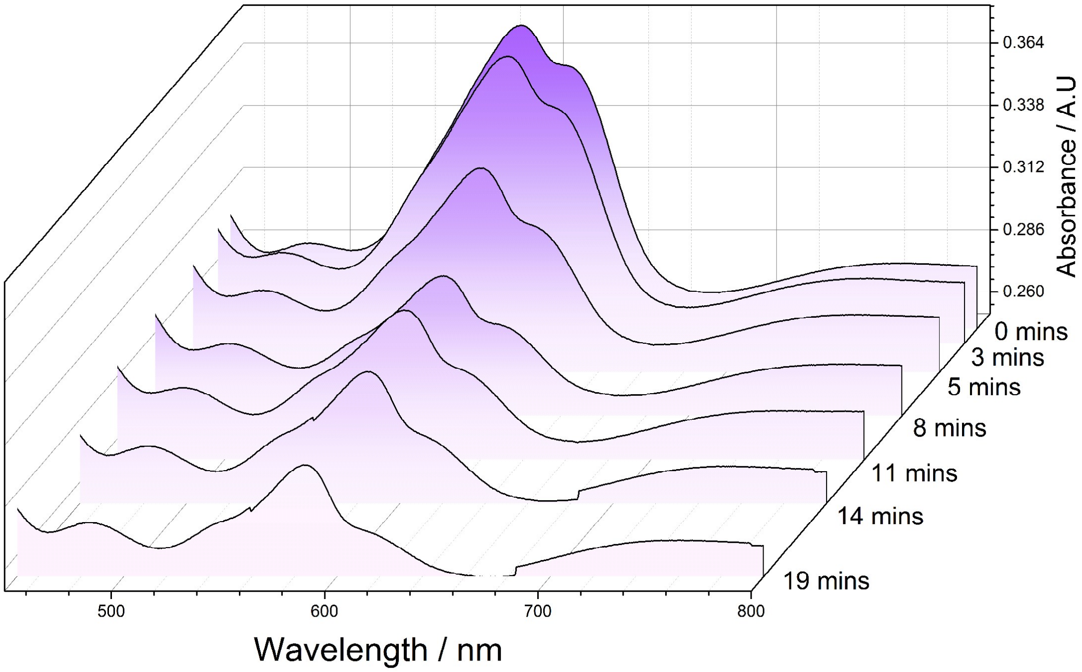

Figure 8: Shows the degradation of resazurin redox dye on the ZrO_2-TiO_2composite thin films by UVA irradiation.

The formal quantum efficiencies (FQE) and formal quantum yields (FQY) for the TiO_2 and ZrO_2-TiO_2 composite films were calculated by taking into account the UVA photon flux on the films and the number of photons absorbed by the films. Figure 9 shows FQE and FQY for the pure TiO_2 and composite films. The FQE for the TiO_2 was 3.3 x 10^{-4} dye molecules destroyed / incident photon and the ZrO_2-TiO_2 composite film was an order of magnitude better at 2 x 10^{-3} dye molecules destroyed / incident photon. The FQY calculated for both films also showed that the composite film (4.9 x 10^{-3} dye molecules destroyed / absorbed photon) was again an order of magnitude better than the pure TiO_2 film (5.1 x 10^{-4} dye molecules destroyed / absorbed photon). The enhanced photocatalytic activity of the composite film compared to the pure TiO_2 film is most likely due to the greater concentration of hydroxyl groups found on the composite surface that amplify surface acidity and reactivity towards pollutants.[31] Furthermore, the superior performance of the ZrO_2-TiO_2 composite in the degradation of resasurin is also helped by the supressed charge carrier recombinations as the surface hydroxyl groups act as hole traps.[31, 32]

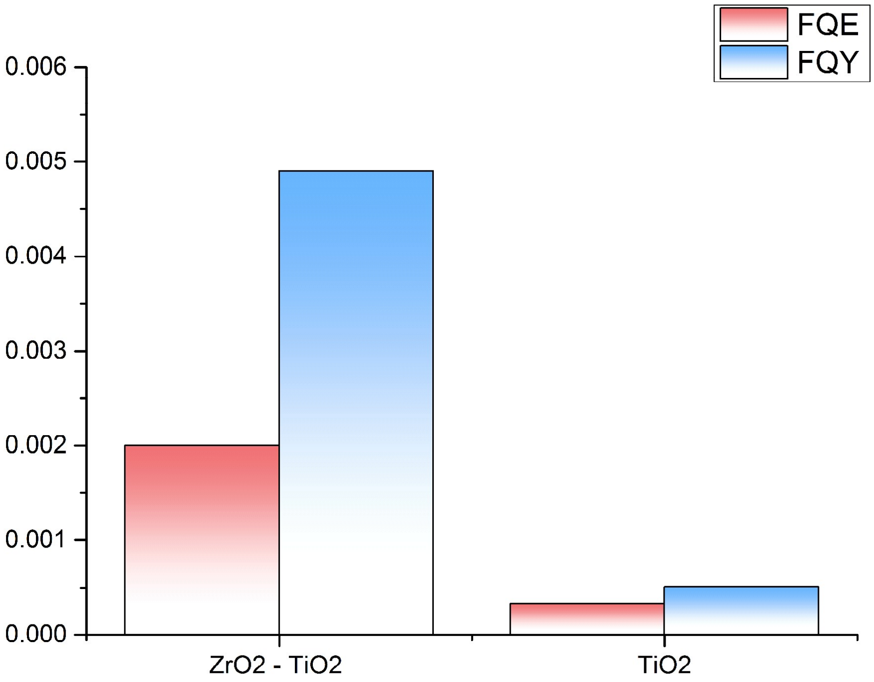

Figure 9: Illustrates the formal quantum efficiency (FQE) and the formal quantum yield (FQY) of the UVA induced photocatalytic reduction of resazurin redox dye for ZrO_2-TiO_2 composite and TiO_2 thin films

3.2.2 Photoinduced wettability

The water contact angle for ZrO_2, TiO_2 and ZrO_2-TiO_2 composite thin films was assessed before and after UVA radiation (flux= 3.67×10^{14} photons per cm^2 per s) for 16 hours by 5 µL droplet of water on the films (see supporting information). There was no significant change in the water contact angle from pre and post irradiation. This is expected for pure ZrO_2 as UVA irradiation is too weak to induce wettability, however literature examples show TiO_2 and ZrO_2-TiO_2 films to be readily activated by UVA resulting in a significant decrease in the post irradiation water contact angle.[48]

4 Conclusions

In this paper we have shown the novel use of AACVD to synthesis a ZrO_2 –TiO_2 composite thin film. The composite film that shows enhanced photocatalytic activity under UVA activation compared to a TiO_2 film (deposited under the same conditions). The enhancement is believed to result from synergistic effects such as improved surface acidity. Further work on the effects of temperature and ratios of TiO_2 and ZrO_2 on the photocatalytic properties are of interest.

5 Acknowledgements

The authors would like to thank Clair Chew and Yao Lu for helpful discussions. We are grateful to King Abdulaziz City for Science and Technology (KACST), Saudi Arabia for the provision of a PhD studentship to Abdullah Alotaibi and for financial support from the Saudi Cultural Bureau in London.

6 References

1. A. L. Linsebigler, G. Lu and J. T. Yates Jr, *Chem. Rev.*, 1995, **95**, 735-758.
2. C. McCullagh, J. M. Robertson, D. W. Bahnemann and P. K. Robertson, *Res. Chem. Intermed.*, 2007, **33**, 359-375.
3. R. Asahi, T. Morikawa, T. Ohwaki, K. Aoki and Y. Taga, *science*, 2001, **293**, 269-271.
4. A. Mills and S. Le Hunte, *Journal of photochemistry and photobiology A: Chemistry*, 1997, **108**, 1-35.
5. D. O. Scanlon, C. W. Dunnill, J. Buckeridge, S. A. Shevlin, A. J. Logsdail, S. M. Woodley, C. R. A. Catlow, M. J. Powell, R. G. Palgrave and I. P. Parkin, *Nat. Mater.*, 2013, **12**, 798-801.
6. K. Hashimoto, H. Irie and A. Fujishima, *Jpn. J. Appl. Phys.*, 2005, **44**, 8269.
7. M. Tasbihi, U. L. Stangar, F. Fresno, N. N. Tusar and D. Barreca, *Journal of Surfaces and Interfaces of Materials*, 2014, **2**, 267-273.
8. T. Luttrell, S. Halpegamage, J. Tao, A. Kramer, E. Sutter and M. Batzill, *Scientific reports*, 2014, **4**.
9. M. Pelaez, N. T. Nolan, S. C. Pillai, M. K. Seery, P. Falaras, A. G. Kontos, P. S. Dunlop, J. W. Hamilton, J. A. Byrne and K. O'Shea, *Applied Catalysis B: Environmental*, 2012, **125**, 331-349.
10. X. Chen and C. Burda, *J. Am. Chem. Soc.*, 2008, **130**, 5018-5019.
11. D. S. Bhachu, S. Sathasivam, C. J. Carmalt and I. P. Parkin, *Langmuir*, 2014, **30**, 624-630.
12. R. Marschall, *Adv. Funct. Mater.*, 2014, **24**, 2421-2440.
13. S. Ponja, S. Sathasivam, N. Chadwick, A. Kafizas, S. M. Bawaked, A. Y. Obaid, S. Al-Thabaiti, S. N. Basahel, I. P. Parkin and C. J. Carmalt, *J. Mater. Chem. A*, 2013, **1**, 6271-6278.
14. S. Sathasivam, A. Kafizas, S. Ponja, N. Chadwick, D. S. Bhachu, S. M. Bawaked, A. Y. Obaid, S. Al-Thabaiti, S. N. Basahel and C. J. Carmalt, *Chem. Vap. Deposition*, 2014, **20**, 69-79.
15. K. Rajeshwar, N. R. de Tacconi and C. R. Chenthamarakshan, *Chem. Mater.*, 2001, **13**, 2765-2782.
16. K. Vinodgopal and P. V. Kamat, *Environmental science & technology*, 1995, **29**, 841-845.
17. S. C. Singhal and K. Kendall, *High-temperature solid oxide fuel cells: fundamentals, design and applications: fundamentals, design and applications*, Elsevier, 2003.
18. C. Tedmon, H. Spacil and S. Mitoff, *J. Electrochem. Soc.*, 1969, **116**, 1170-1175.
19. J. H. Shim, C.-C. Chao, H. Huang and F. B. Prinz, *Chem. Mater.*, 2007, **19**, 3850-3854.
20. A. Azad, S. Akbar, S. Mhaisalkar, L. Birkefeld and K. Goto, *J. Electrochem. Soc.*, 1992, **139**, 3690-3704.
21. W.-J. Qi, R. Nieh, B. H. Lee, L. Kang, Y. Jeon and J. C. Lee, *Appl. Phys. Lett.*, 2000, **77**, 3269-3271.
22. S. L. Jangra, K. Stalin, N. Dilbaghi, S. Kumar, J. Tawale, S. P. Singh and R. Pasricha, *J. Nanosci. Nanotechnol.*, 2012, **12**, 7105-7112.
23. M. Shane and M. Mecartney, *J. Mater. Sci.*, 1990, **25**, 1537-1544.
24. J. Kim and Y. Lin, *J. Membr. Sci.*, 1998, **139**, 75-83.
25. R. Piticescu, C. Monty, D. Taloi, A. Motoc and S. Axinte, *J. Eur. Ceram. Soc.*, 2001, **21**, 2057-2060.
26. R. Thomas, A. Milanov, R. Bhakta, U. Patil, M. Winter, P. Ehrhart, R. Waser and A. Devi, *Chem. Vap. Deposition*, 2006, **12**, 295-300.
27. P. A. Williams, J. L. Roberts, A. C. Jones, P. R. Chalker, N. L. Tobin, J. F. Bickley, H. O. Davies, L. M. Smith and T. J. Leedham, *Chem. Vap. Deposition*, 2002, **8**, 163-170.
28. J. Gottmann and E. Kreutz, *Surf. Coat. Technol.*, 1999, **116**, 1189-1194.
29. D. Fork, D. Fenner, G. Connell, J. M. Phillips and T. Geballe, *Appl. Phys. Lett.*, 1990, **57**, 1137-1139.
30. D. Prakashbabu, R. Hari Krishna, B. M. Nagabhushana, H. Nagabhushana, C. Shivakumara, R. P. S. Chakradar, H. B. Ramalingam, S. C. Sharma and R. Chandramohan, *Spectrochimica Acta Part A: Molecular and Biomolecular Spectroscopy*, 2014, **122**, 216-222.

31. X. Fu, L. A. Clark, Q. Yang and M. A. Anderson, *Environmental Science & Technology*, 1996, **30**, 647-653.
32. J. C. Yu, J. Lin and R. W. M. Kwok, *The Journal of Physical Chemistry B*, 1998, **102**, 5094-5098.
33. D. S. Bhachu, D. O. Scanlon, G. Sankar, T. D. Veal, R. G. Egdell, G. Cibin, A. J. Dent, C. E. Knapp, C. J. Carmalt and I. P. Parkin, *Chem. Mater.*, 2015, **27**, 2788-2796.
34. D. S. Bhachu, D. O. Scanlon, E. J. Saban, H. Bronstein, I. P. Parkin, C. J. Carmalt and R. G. Palgrave, *J. Mater. Chem. A*, 2015, **3**, 9071-9073.
35. S. Sathasivam, R. R. Arnepalli, B. Kumar, K. K. Singh, R. J. Visser, C. S. Blackman and C. J. Carmalt, *Chem. Mater.*, 2014, **26**, 4419-4424.
36. D. S. Bhachu, S. Sathasivam, G. Sankar, D. O. Scanlon, G. Cibin, C. J. Carmalt, I. P. Parkin, G. W. Watson, S. M. Bawaked, A. Y. Obaid, S. Al-Thabaiti and S. N. Basahel, *Adv. Funct. Mater.*, 2014, **24**, 5075-5085.
37. S. Sathasivam, D. S. Bhachu, Y. Lu, N. Chadwick, S. A. Althabaiti, A. O. Alyoubi, S. N. Basahel, C. J. Carmalt and I. P. Parkin, *Scientific reports*, 2015, **5**.
38. P. Marchand, I. A. Hassan, I. P. Parkin and C. J. Carmalt, *Dalton Trans.*, 2013, **42**, 9406-9422.
39. C. Anderson and A. J. Bard, *The Journal of Physical Chemistry*, 1995, **99**, 9882-9885.
40. L. Liang, Y. Sheng, Y. Xu, D. Wu and Y. Sun, *Thin Solid Films*, 2007, **515**, 7765-7771.
41. A. Mills, J. Wang, S.-K. Lee and M. Simonsen, *Chemical communications*, 2005, 2721-2723.
42. S. J. S. Qazi, A. R. Rennie, J. K. Cockcroft and M. Vickers, *J. Colloid Interface Sci.*, 2009, **338**, 105-110.
43. P. E. Lippens, A. V. Chadwick, A. Weibel, R. Bouchet and P. Knauth, *The Journal of Physical Chemistry C*, 2008, **112**, 43-47.
44. S.-m. Chang and R.-a. Doong, *The Journal of Physical Chemistry B*, 2006, **110**, 20808-20814.
45. T. Ohsaka, F. Izumi and Y. Fujiki, *J. Raman Spectrosc.*, 1978, **7**, 321-324.
46. A. Kafizas and I. P. Parkin, *J. Am. Chem. Soc.*, 2011, **133**, 20458-20467.
47. C. Morant, J. M. Sanz, L. Galán, L. Soriano and F. Rueda, *Surf. Sci.*, 1989, **218**, 331-345.
48. W. Zhou, K. Liu, H. Fu, K. Pan, L. Zhang, L. Wang and C.-c. Sun, *Nanotechnology*, 2008, **19**, 035610.